DOI: 10.1002/ejic.200600256

Silica Supported Submicron $SiO_2@Y_2SiO_5:Eu^{3+}$ and $SiO_2@Y_2SiO_5:Ce^{3+}/Tb^{3+}$ Spherical Particles with a Core–Shell Structure: Sol–Gel Synthesis and Characterization

Cuikun Lin,[a] Huan Wang,[b] Deyan Kong,[a] Min Yu,[b] Xiaoming Liu,[a] Zhenling Wang,[a] and Jun Lin*[a]

Keywords: Sol–gel processes / Luminescence / Core–shell structures / Silicates / Materials science

X_1-$Y_2SiO_5:Eu^{3+}$ and X_1-$Y_2SiO_5:Ce^{3+}$ and/or Tb^{3+} phosphor layers have been coated on nonaggregated, monodisperse, submicron spherical SiO_2 particles by a sol–gel process, followed by surface reaction at high temperature (1000 °C), to give core/shell structured $SiO_2@Y_2SiO_5:Eu^{3+}$ and $SiO_2@Y_2SiO_5:Ce^{3+}/Tb^{3+}$ particles. X-ray diffraction (XRD), field emission scanning electron microscopy (FESEM), TEM, photoluminescence (PL), low voltage cathodoluminescence (CL), and time-resolved PL spectra and lifetimes are used to characterize these materials. The XRD results indicate that X_1-Y_2SiO_5 layers have been successfully coated on the surface of SiO_2 particles, as further verified by the FESEM and TEM images. The PL and CL studies suggest that $SiO_2@Y_2SiO_5:Eu^{3+}$, $SiO_2@Y_2SiO_5:Tb^{3+}$ (or Ce^{3+}/Tb^{3+}), and $SiO_2@Y_2SiO_5:Ce^{3+}$ core/shell particles exhibit red (Eu^{3+}, 613 nm: $^5D_0$–$^7F_2$), green (Tb^{3+}, 542 nm: $^5D_4$–$^7F_5$), or blue (Ce^{3+}, 450 nm: 5d-4f) luminescence, respectively. PL excitation, emission, and time-resolved spectra demonstrate that there is an energy transfer from Ce^{3+} to Tb^{3+} in the $SiO_2@Y_2SiO_5:Ce^{3+},Tb^{3+}$ core/shell particles.

Introduction

The synthesis of nanostructured inorganic materials with hierarchical morphologies has attracted considerable attention in the fields of catalysis, separation technology, microelectronic devices, and biomaterials engineering.[1] In particular, the term core/shell nowadays comprises a huge area of particles that are in the broadest sense defined by a core of matter that is surrounded by a shell of different matter.[2] Core/shell materials can be used to protect drugs or other materials from dissolving or hydrolysis and to strength polymeric materials,[3] and a gold core has been found to act as an antenna that absorbs light that is then transferred to a bound rare-earth oxide shell, thereby enhancing the oxide luminescence.[4] There are numerous methods for preparing core/shell structured materials, including vapor deposition, plasma-assisted techniques, chemical reduction, self-assembly, and co-precipitation.[5] In most cases, however, the degree of surface coverage is low and the coating is not uniform.[6] The sol–gel process is an effective method for preparing such materials since the reactants can be homogeneously mixed at molecular level in solution.

The current demand for high-resolution, high brightness, and high efficiency in phosphors for cathode-ray tubes, field-emissive displays, and plasma display panels has promoted the development of new phosphors, particularly those with a nonagglomerated, monodisperse, spherical (<2 μm) morphology as they offer higher packing density, lower scattering of light, brighter luminescent performance, higher definition, and more improved screen packing.[7] Nowadays, many synthetic routes have been developed to control the size, morphology, and distribution of phosphor particles, such as spray pyrolysis[8] and flux precipitation,[9] but it is still difficult to obtain highly monodisperse and spherical phosphor particles by these methods.

It is well known that monodisperse and spherical silica particles in the nano- to submicron range can be prepared by the hydrolysis and condensation of tetraethoxysilane (TEOS) catalyzed by ammonia.[10] If the silica spheres are coated with phosphors layers, a kind of core/shell phosphor material with spherical morphology will be obtained and the size of the phosphor particles can be controlled by the silica cores. Furthermore, because silica is cheaper than most of the phosphor materials, which often employ expensive rare-earth elements as activators and/or host components, core/shell phosphor materials should be cheaper than the pure phosphor materials. Y_2SiO_5 is an important material that shows many interesting properties, and rare-earth (RE) oxyorthosilicates [$(RE)_2SiO_5$] doped with Eu^{3+},

[a] Key laboratory of Rare Earth Chemistry and Physics, Changchun Institute of Applied Chemistry, Chinese Academy of Sciences, Changchun 130022; and Graduate School of the Chinese Academy of Sciences,
Beijing 100049, P. R. China
Fax: +86-431-569-8041
E-mail: jlin@ns.ciac.jl.cn
[b] Department of Chemistry, Northeast Normal University, Changchun 130024, P. R. China
Supporting information for this article is available on the WWW under http://www.eurjic.org or from the author.

Ce^{3+}, and Tb^{3+} are well-known luminescent materials.[11–13] It is well known that Y_2SiO_5 is a good laser host[14] and Y_2SiO_5:Tb is one of the best green-emitting cathodoluminescent phosphors.[15] Y_2SiO_5:Eu has also been found to be a promising candidate for coherent time-domain optical memory (CTDOM) applications.[16] Therefore, rare-earth-doped yttrium orthosilicates have been attracting the attention of many research groups.

In this paper, we employ monodisperse SiO_2 spheres as supporting cores to prepare $SiO_2@Y_2SiO_5:Eu^{3+}$ and $SiO_2@Y_2SiO_5:Ce^{3+}/Tb^{3+}$ core/shell-structured phosphor particles by a sol–gel process, and thoroughly characterize the structure, morphology, and luminescent properties of these samples.

Results and Discussion

The procedures for preparation of monodisperse core/shell-structured $SiO_2@Y_2SiO_5:Eu^{3+}$ and $SiO_2@Y_2SiO_5:Ce^{3+}/Tb^{3+}$ submicron spherical particles together with their luminescence photos are given in Figure S1 (see Supporting Information). The synthesis of the monodisperse SiO_2 core particles was carried out by the well-known Stöber method, i.e., hydrolysis of TEOS in an ethanol solution containing water and ammonia.[10] This process yielded a colloidal solution of silica particles with a narrow size distribution in the submicron range, with the particle size of silica dependent on the relative concentration of the reactants. A sol–gel technique was used for the deposition of the $Y_2SiO_5:Eu^{3+}$ and $Y_2SiO_5:Ce^{3+}/Tb^{3+}$ shells on the SiO_2 cores to produce core/shell-structured $SiO_2@Y_2SiO_5:Eu^{3+}$ and $SiO_2@Y_2SiO_5:Ce^{3+}/Tb^{3+}$ particles.

Formation and Morphology of Core–Shell Particles

The formation and morphology of the core/shell particles were performed representatively for $SiO_2@Y_{1.9}Tb_{0.1}SiO_5$ by X-ray diffraction (XRD), field emission scanning electron microscopy (FESEM), and TEM. The results for the other compounds were similar to those of $SiO_2@Y_{1.9}Tb_{0.1}SiO_5$ and will not be discussed further.

The oxyorthosilicates $(RE)_2SiO_5$ of the larger rare-earth ions (RE = La–Tb) possess a monoclinic X_1-type structure with the space group $P2_1/C$ (no. 14),[17] whereas the smaller ones (RE = Dy–Lu, Sc) have an X_2-type structure with the space group $B2/b$ (no. 15).[18] Y_2SiO_5 crystallizes in the X_1 structure when annealed at a temperature below 1190 °C and in the X_2 structure above this temperature.[19] Figure S2 (Supporting Information) shows the structure of X_1-Y_2SiO_5. This structure contains isolated SiO_4 tetrahedra and nonsilicon-bonded oxygen. There are two types of Y positions. Y1 is coordinated by nine oxygen atoms, eight of which are bonded to silicon, and Y2 is coordinated by seven atoms, four of which are bonded to silicon.[20]

Figure 1 shows the XRD profiles for the pure $Y_{1.9}Tb_{0.1}SiO_5$ powder (a) and $SiO_2@Y_{1.9}Tb_{0.1}SiO_5$ (b), both annealed at 1000 °C, as well as the JCPDS 21-1456 card for X_1-Y_2SiO_5 (c) as the reference. For the $SiO_2@Y_{1.9}Tb_{0.1}SiO_5$ sample (Figure 1, b), besides the broad band at $2\theta = 22°$ due to amorphous SiO_2,[7] all the diffraction peaks can be indexed according to the standard data of X_1-Y_2SiO_5 (JCPDS 21-1456). This agrees well with the pure $Y_{1.9}Tb_{0.1}SiO_5$ powder sample annealed at 1000 °C, which also crystallizes with the X_1-Y_2SiO_5 phase structure. No second phase was detected. In general, the nanocrystallite size can be estimated from the Scherrer formula: $D_{hkl} = K\lambda/(\beta\cos\theta)$, where λ is the X-ray wavelength (0.15405 nm), β is the full-width at half-maximum, θ is the diffraction angle, K is a constant (0.89), and D_{hkl} is the size along the (hkl) direction.[21] Here, we use diffraction data at 29.60°, 31.02°, 32.58°, and 33.64° to calculate the crystallite size, which give an estimated average crystallite size of 22 nm for $Y_{1.9}Tb_{0.1}SiO_5$ on the SiO_2 sphere and 29 nm for pure $Y_{1.9}Tb_{0.1}SiO_5$. The unit cell parameters and crystallite size of Y_2SiO_5 powder and $SiO_2@Y_{1.9}Tb_{0.1}SiO_5$ core/shell particles, as well as the internuclear distances and angles of the $SiO_2@Y_{1.9}Tb_{0.1}SiO_5$ core/shell particles, were calculated using Jade 5.0 and CASTEP,[22] respectively. The results are listed in Table 1 and Table S1, respectively.

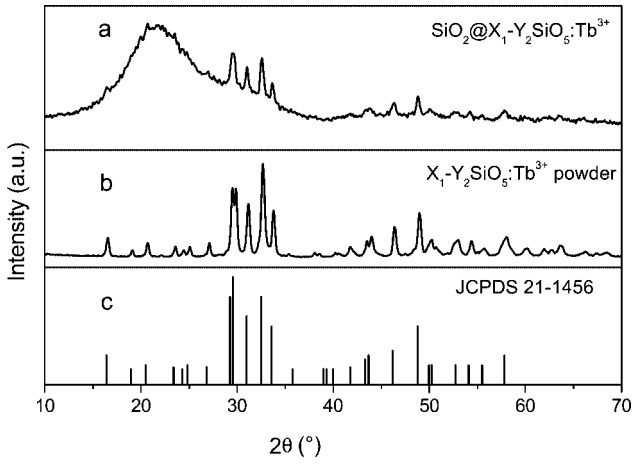

Figure 1. XRD patterns of $SiO_2@Y_{1.9}Tb_{0.1}SiO_5$ (a) and $SiO_2@Y_{1.9}Tb_{0.1}SiO_5$ (b) particles annealed at 1000 °C as well as the standard data for JCPDS No. 21-1456 (c) as a reference.

Table 1. Calculated unit-cell parameters and crystalline size of Y_2SiO_5 powder and $SiO_2@Y_2SiO_5$:Tb core/shell particles.

Sample	*a* [nm]	*b* [nm]	*c* [nm]	*β* [°]	Crystal size [nm]
Y_2SiO_5 powder	0.905	0.690	0.664	106.41	29
$SiO_2@Y_2SiO_5$:Tb core/shell particles	0.899	0.694	0.662	106.48	22

Figure 2 shows the SEM micrographs of the as-formed SiO_2 particles (a) and $SiO_2@Y_{1.9}Tb_{0.1}SiO_5$ (coated four times) core/shell particles (b). From the SEM micrograph in Figure 2 (see part a), we can see that the as-formed SiO_2 sample consists of spherical particles with an average size of 385 nm and that these particles are nonaggregated and have a narrow size distribution. After functionalizing the silica particles by coating four times with $Y_{1.9}Tb_{0.1}SiO_5$, the

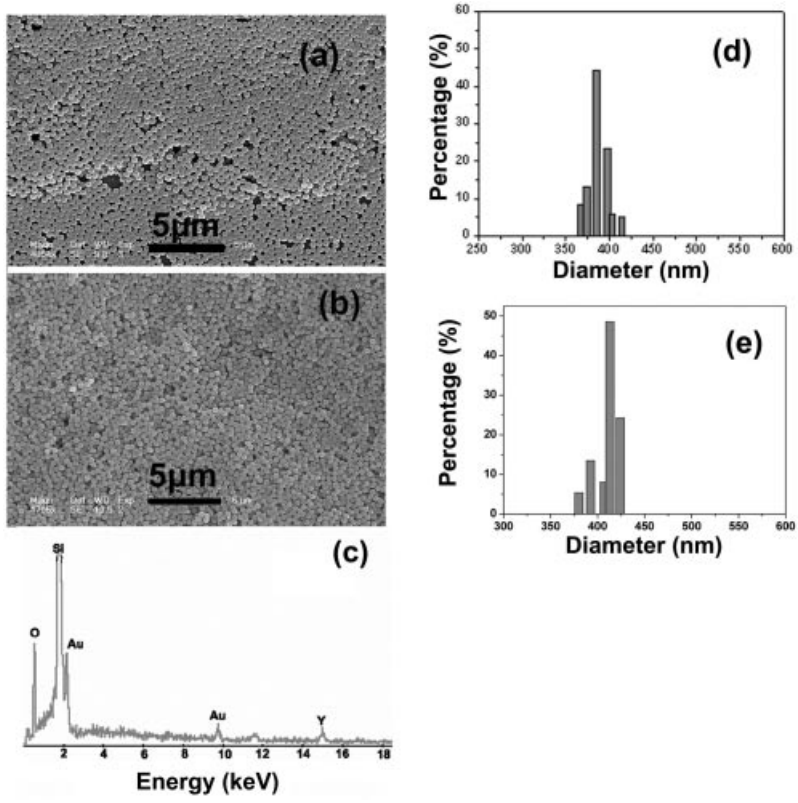

Figure 2. FESEM micrographs of amorphous SiO_2 (a) and core/shell-structured $SiO_2@Y_{1.9}Tb_{0.1}SiO_5$ particles (b) as well as the histograms for their size distribution (d for a, e for b) and EDX analysis of the core/shell-structured $SiO_2@Y_{1.9}Tb_{0.1}SiO_5$ particles (c).

resultant $SiO_2@Y_{1.9}Tb_{0.1}SiO_5$ particles are still spherical and uniform and keep the morphological properties of the silica particles, as shown in Figure 2 (b). The mean size of these particles is about 413 nm, which is a little larger than pure silica. The core/shell spheres were examined by energy-dispersive X-ray (EDX) analysis, which confirmed the presence of Y, Si, and O on the surface (Figure 2, c). Tb was not detected due to its low concentration, although it can be detected in the luminescence spectra (see below).

In order to investigate the inner structure of $SiO_2@Y_{1.9}Tb_{0.1}SiO_5$, TEM was performed. Figure 3 shows the SiO_2 particles coated by four layers of $Y_{1.9}Tb_{0.1}SiO_5$ shells; the core/shell structure of the sample can be seen clearly due to the different electron penetrability of the core and shell. The core can be seen as a black sphere with an average size of 350 nm and the shells have a gray color and an average thickness of 50 nm. Electron diffraction measurements were performed at the interface region of the core and shell of a particle, as shown in the inset of Figure 3 (b). The electron-diffraction rings demonstrate the existence of a crystalline phase at the surface of the core/shell particles.

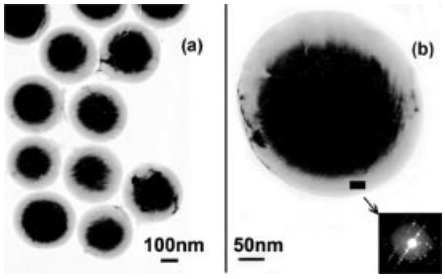

Figure 3. TEM micrographs of $SiO_2@$ $Y_{1.9}Tb_{0.1}SiO_5$ (a, b). The inset in (b) is the electron-diffraction pattern of the selected region.

Photoluminescence Properties

The as-prepared core/shell particles of $SiO_2@Y_2SiO_5:Eu^{3+}$, $SiO_2@Y_2SiO_5:Tb^{3+}$ (or Ce^{3+}/Tb^{3+}), and $SiO_2@Y_2SiO_5:Ce^{3+}$ can be dispersed in solvents such as ethanol and water to form a relatively stable colloidal solution. Under UV excitation, these colloidal solutions show bright red ($SiO_2@Y_2SiO_5:Eu^{3+}$), blue ($SiO_2@Y_2SiO_5:Ce^{3+}$), and green ($SiO_2@Y_2SiO_5:Tb^{3+}$ and $SiO_2@Y_2SiO_5:Ce^{3+},Tb^{3+}$) luminescence, as shown in Figure S1.

$SiO_2@Y_2SiO_5:Eu^{3+}$

$SiO_2@Y_2SiO_5:Eu^{3+}$ core/shell particles exhibit a strong red emission under UV irradiation. Figure 4 (a) shows the excitation and emission spectra of $SiO_2@Y_{1.8}Eu_{0.2}SiO_5$ core/shell particles. The excitation spectrum (Figure 4, part a, left) consists of a broad, intense band, with a maximum at 253 nm, and some weak lines. The former is due to the charge-transfer band (CTB) of Eu^{3+}–O^{2-}, and the latter are

due to f-f transitions within the Eu^{3+} $4f^6$ electron configuration (320: $^7F_0 \rightarrow {}^5H_6$; 364: $^7F_0 \rightarrow {}^5D_4$; 384: $^7F_0 \rightarrow {}^5G_2$; 397: $^7F_0 \rightarrow {}^5L_6$, 468: $^7F_0 \rightarrow {}^5D_2$).[23] Upon excitation into the CTB at 253 nm, the emission spectrum was found to be composed of $^5D_0 \rightarrow {}^7F_J$ (J = 0, 1, 2, 3, 4) emission lines of Eu^{3+}, with the hypersensitive red emission $^5D_0 \rightarrow {}^7F_2$ (612 nm) transition being the most prominent group (Figure 6, part a, right). When the Eu^{3+} is located at a low-symmetry local site (without an inversion center), the hypersensitive $^5D_0 \rightarrow {}^7F_2$ transition is often dominant in its emission spectrum.[24] This is actually the case for X_1-Y_2SiO_5, which adopts a monoclinic structure with a space group of $P2_1/c$ where the two Y^{3+} sites have a C_1 point symmetry (without an inversion center).[12,24] The doped Eu^{3+} ions occupy the Y^{3+} sites in the $SiO_2@X_1$-Y_2SiO_5 core/shell particles, which results in the hypersensitive red emission $^5D_0 \rightarrow {}^7F_2$ transition of Eu^{3+} being the most prominent group in its emission spectrum.

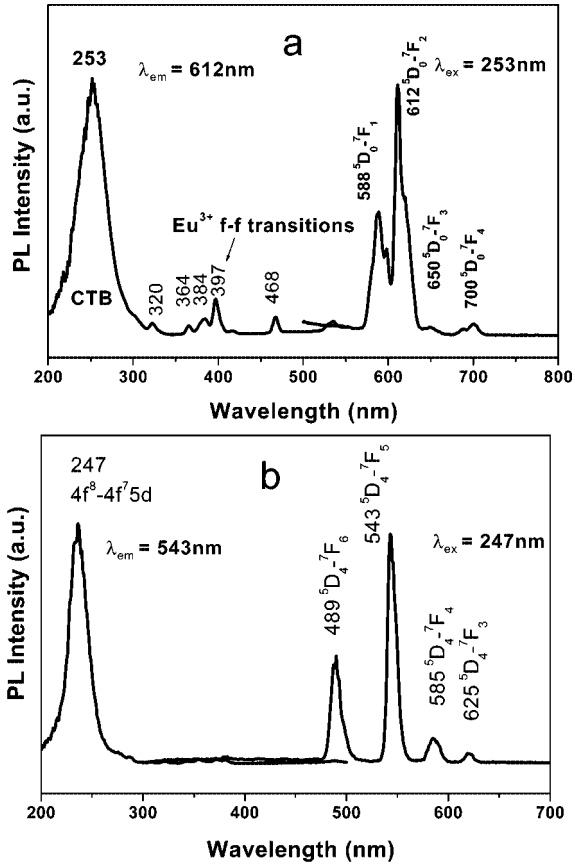

Figure 4. Excitation (left) and emission (right) spectra for $SiO_2@Y_{1.8}Eu_{0.2}SiO_5$ core/shell particles (a) and excitation (left) and emission (right) spectra for $SiO_2@Y_{1.9}Tb_{0.1}SiO_5$ core/shell particles (b).

The decay curve for the $^5D_0 \rightarrow {}^7F_2$ transition of Eu^{3+} in $SiO_2@Y_{1.8}Eu_{0.2}SiO_5$ core/shell particles is shown in Figure S3; it can be well fitted to a single-exponential function as $I = A\exp(-\tau/\tau_0)$[25] (the fitting parameters are shown in the figure). A lifetime, τ, of 2.31 ms is obtained for the $^5D_0 \rightarrow {}^7F_2$ emission of Eu^{3+}.

Because of the invariability of the Eu^{3+} $^5D_0 \rightarrow {}^7F_1$ transition intensity, it can be taken as a reference for the calculation of luminescent quantum yield.[26,27] On obtaining the intensity parameters of the Eu^{3+} emission spectra, the total radiative rate of $^5D_0$ can be expressed by Equation (1),[27,28]

$$k_r = k_{r(0-1)} \frac{\sum_{J=0}^{4} S_{(0-J)}}{S_{(0-1)}} \quad (1)$$

where $S_{(0\rightarrow J)}$ and $S_{(0\rightarrow 1)}$ are the integral intensities of the $^5D_0 \rightarrow {}^7F_J$ and $^5D_0 \rightarrow {}^7F_1$ transitions, respectively, and $k_{r(0\rightarrow 1)}$ is the radiative rate of the $^5D_0 \rightarrow {}^7F_1$ transition. Since $[k_{r(0\rightarrow 1)}]_{vac}$ is 14.65 s^{-1},[29] when an average index of refraction, n, equal to 1.506 is considered, the value of k_{0-1} is equal to $n^3[k_{r(0\rightarrow 1)}]_{vac}$, about 50 s^{-1}.[26,29–32]

The total radiative rate of $^5D_0$ was determined to be 0.137 ms^{-1} from Equation (1). All the $^5D_0$ decay curves determined for the samples could be fitted well to a single-exponential function, which reflects the existence of the Eu^{3+} local site symmetry.[33,34] The fitted lifetime is 2.31 ms. From these data, the total decay rate of $^5D_0$ (K_{tot}), which can be given as Equation (2), is 0.433 ms^{-1}. Finally, the absolute emission quantum yield (η) determined from Equation (3) is around 32%. This quantum value seems rather low considering that the materials have been annealed at 1000 °C, which generally leads to high quantum yields for this rare-earth ion. This may be due to the concentration quenching effect. It should be noted that Equation (3) describes the quantum efficiency of the Eu^{3+} $^5D_0$ level and not the absolute emission quantum yield of the $SiO_2@Y_2SiO_5$:Eu^{3+} core/shell particles, and that the absolute emission quantum yield is a more general quantity that involves the ratio between light absorption and light emission. Therefore, the absolute emission quantum yield and the quantum efficiency of the $^5D_0$ level are equal if all the energy absorbed is transferred to the $^5D_0$ level.

$$k_{tot} = \frac{1}{\tau} = k_r + k_{nr} \quad (2)$$

$$\eta = \frac{k_r}{k_r + k_{nr}} \quad (3)$$

$SiO_2@Y_2SiO_5$:Tb^{3+}

$SiO_2@Y_2SiO_5$:Tb^{3+} core/shell particles exhibit a strong green emission under UV irradiation. Figure 4 (b) shows the excitation and emission spectra of $SiO_2@Y_{1.9}Tb_{0.1}SiO_5$ core/shell particles. The excitation spectrum (Figure 4, part b, left) contains an intense, broad band with a maximum at 247 nm due to the spin-allowed $4f^8 \rightarrow 4f^75d$ transition (ΔS = 0) of Tb^{3+}.[34] The excitation lines in the longer wavelength regions within the Tb^{3+} $4f^8$ electron configuration cannot be seen at this magnification due to their weak intensity.

Excitation into the spin-allowed $4f^8 \rightarrow 4f^7 5d$ band at 247 nm yields the characteristic emission lines of Tb^{3+} $^5D_4 \rightarrow {}^7F_J$ (J = 3, 4, 5, 6) transitions, with the $^5D_4 \rightarrow {}^7F_5$ (543 nm) green emission as the most prominent group (Figure 4, part b, right).

The decay curve for $^5D_4 \rightarrow {}^7F_5$ of Tb^{3+} in $SiO_2@Y_{1.9}Tb_{0.1}SiO_5$ core/shell particles is shown in Figure S4, which can also be well fitted to a single-exponential function like the situation for Eu^{3+} in $SiO_2@Y_{1.8}Eu_{0.2}SiO_5$; the fitting parameters are shown in the figure. A lifetime value of 3.29 ms is obtained for the $^5D_4 \rightarrow {}^7F_5$ emission of Tb^{3+}.

The PL intensity of $SiO_2@Y_{1.9}Tb_{0.1}SiO_5$ core/shell particles can be tuned by the number of coatings. Figure 5 shows the PL intensity of the sample as a function of the coating number. Obviously, the PL intensity increases with an increase of coating number, which can be attributed to an increase of the thickness of the $Y_{1.9}Tb_{0.1}SiO_5$ shells on the SiO_2 spheres. The PL intensity of the four-layer $SiO_2@Y_{1.9}Tb_{0.1}SiO_5$ core/shell particles reaches about 62% of that of the pure $Y_{1.9}Tb_{0.1}SiO_5$ sample, as indicated in Figure 5.

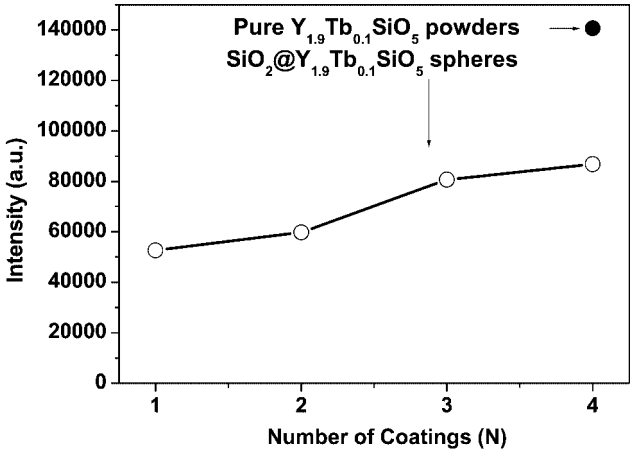

Figure 5. The photoluminescence intensity of Tb^{3+} as a function of the number of coatings (N) of $SiO_2@Y_{1.9}Tb_{0.1}SiO_5$ core/shell particles. The photoluminescence intensity of pure $Y_{1.9}Tb_{0.1}SiO_5$ is also given for comparison.

$SiO_2@Y_2SiO_5:Ce^{3+}$ and $SiO_2@Y_2SiO_5:Ce^{3+},Tb^{3+}$

The $SiO_2@Y_2SiO_5:Ce^{3+}$ core/shell particles show a blue emission under longer wavelength UV excitation. The excitation (a) and emission (b) spectra of $SiO_2@Y_{1.94}Ce_{0.06}SiO_5$ core/shell particles are shown in Figure 6. The excitation spectrum mainly consists of a strong band with a maximum at 370 nm and a weak band at 282 nm, corresponding to the transitions from the ground state $^2F_{5/2}$ to the excited 5d states of Ce^{3+}. The emission of Ce^{3+} includes a broad band with a maximum at 443 nm, which is assigned to the parity-allowed transitions of the lowest component of the 5d state to the ground state of Ce^{3+}.[35]

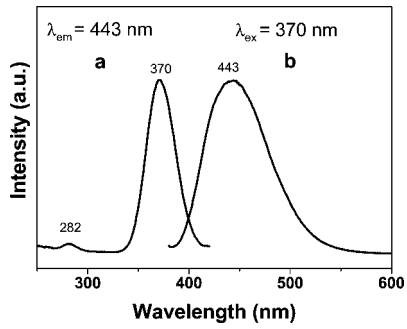

Figure 6. Excitation (a) and emission (b) spectra for SiO_2 @ $Y_{1.94}Ce_{0.06}SiO_5$ core/shell particles.

$SiO_2@Y_{1.84}Ce_{0.06}Tb_{0.1}SiO_5$ core/shell particles show a blue-green emission under UV excitation. The excitation spectrum monitored with the 543 nm emission ($^5D_4 \rightarrow {}^7F_5$) of Tb^{3+} contains an intense band at 247 nm, a weak band at 282 nm, and a strong band with a maximum at 370 nm. By comparison with the excitation spectra for $SiO_2@Y_{1.9}Tb_{0.1}SiO_5$ (Figure 4, b) and $SiO_2@Y_{1.94}Ce_{0.06}SiO_5$ (Figure 5), we can easily ascribe the former band at 247 nm to the $4f^8 \rightarrow 4f^7 5d$ transitions of Tb^{3+}, and the latter bands at 282 and 370 nm to 4f–5d transitions of Ce^{3+} in Figure 7 (a). The presence of the excitation bands of Ce^{3+} in the excitation spectrum monitored with Tb^{3+} emission indicates that an energy transfer has occurred from Ce^{3+} to Tb^{3+} in the $SiO_2@Y_{1.84}Ce_{0.06}Tb_{0.1}SiO_5$ sample. Excitation into the Ce^{3+} excitation band at 370 nm yields both the emission of Ce^{3+} (380–470 nm, which is identical to the emission spectrum of $SiO_2@Y_{1.94}Ce_{0.06}SiO_5$ core/shell particles, dotted line) and that of Tb^{3+} ($^5D_4 \rightarrow {}^7F_J$ at 488, 543, 586, 625 nm), as shown in Figure 7 (b), and is further indicative of the energy transfer from Ce^{3+} to Tb^{3+} in $SiO_2@Y_{1.84}Ce_{0.06}Tb_{0.1}SiO_5$.

The kinetic decay curves for the emission of Ce^{3+} in $SiO_2@Y_{1.94}Ce_{0.06}SiO_5$ and in $SiO_2@Y_{1.84}Ce_{0.06}Tb_{0.1}SiO_5$ were also measured (see Supporting Information, Figure S4, parts a and b, respectively). Both of the decay curves for Ce^{3+} can be well-fitted to a single-exponential function, and the lifetimes (τ) for Ce^{3+} were determined to be 39.8 ns in the former and 20.1 ns in the latter. The shortening of the lifetime in $SiO_2@Y_{1.94}Ce_{0.06}SiO_5$ with respect to $SiO_2@Y_{1.84}Ce_{0.06}Tb_{0.1}SiO_5$ is due to the occurrence of the energy transfer from Ce^{3+} to Tb^{3+} in the latter sample. The $Ce^{3+} \rightarrow Tb^{3+}$ energy transfer is not complete due to the presence of the strong Ce^{3+} emission. The energy-transfer efficiency from a donor (Ce^{3+}) to an acceptor (Tb^{3+}) can be calculated according to the formula $\eta_{ET} = 1 - I_d/I_{d0}$ (= $1 - \tau/\tau_0$), where I_d (τ) and I_{d0} (τ_0) are the corresponding luminescence intensities (lifetimes) of the donor (Ce^{3+}) in the presence and absence of the acceptor (Tb^{3+}) for the same donor concentration, respectively.[36] The energy-transfer efficiency from Ce^{3+} to Tb^{3+} is 48%, as calculated from the lifetimes of Ce^{3+}.

In order to study the energy-transfer process from Ce^{3+} to Tb^{3+} in $SiO_2@Y_{1.84}Ce_{0.06}Tb_{0.1}SiO_5$ in more detail, the time-resolved emission spectra were measured by excitation

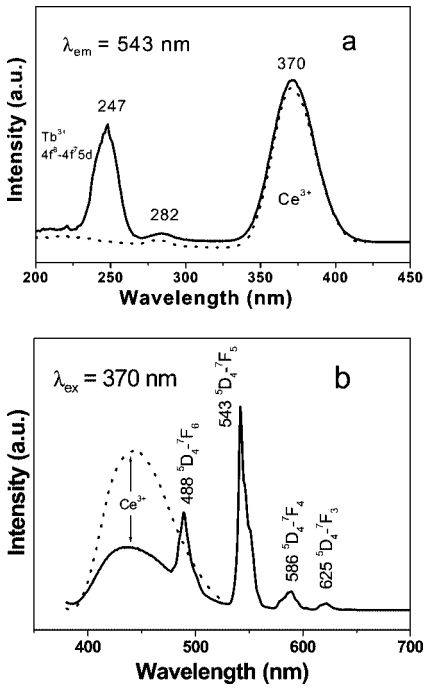

Figure 7. Excitation (a) and emission (b) spectra for $SiO_2@Y_{1.84}Ce_{0.06}Tb_{0.1}SiO_5$ core/shell particles.

into the Ce^{3+} band with a 370-nm laser. The emission spectra collected at different delay times t are shown in Figure 8. When t = 0.25 μs, only the broad emission of Ce^{3+} is observed; no Tb^{3+} emission is present because the excitation energy of Ce^{3+} has not been transferred to Tb^{3+} within this short time. When t = 1.25 μs, the emission of Ce^{3+} starts to decreases and is accompanied by a Tb^{3+} emission due to the energy transfer from Ce^{3+}. The emission of Ce^{3+} decreases gradually with further increase of the delay time, while that of Tb^{3+} begins to increase (a large part of the Tb^{3+} emission is from the $^5D_3$ level) due to transfer of more excitation energy from Ce^{3+} to Tb^{3+}. When t = 7.75 μs, the emission of Ce^{3+} disappears, and the emission spectrum contains exclusively that of Tb^{3+}. The emission from the $^5D_3$ level of Tb^{3+} then begins to decrease until it is quenched completely at t = 100 μs. This quenching of the $^5D_3$ emission of Tb^{3+} is due to cross-relaxation between two adjacent Tb^{3+} ions, i.e. Tb^{3+} ($^5D_3$) + Tb^{3+} ($^7F_6$) → Tb^{3+} ($^5D_4$) + Tb^{3+} ($^7F_0$), which occurs at a longer delay time.[36]

The mechanism of nonradiative energy transfer from Ce^{3+} (5d-level) to Tb^{3+} (mainly the $^5D_3$ level) is an inductive resonant process. Since the concentration of Ce^{3+} ions is not great, a dipole–dipole interaction between Ce^{3+} and Tb^{3+} in the excited state is the most likely one.[37,38] The absolute constant of the energy-transfer rate can be defined by the formula $K_t = 1/\tau - 1/\tau_0$, where τ and τ_0 are the decay times of luminescence for the donor ions with and without the acceptor, respectively.[38,39] So, for $SiO_2@Y_{1.84}Ce_{0.06}Tb_{0.1}SiO_5$, the energy-transfer rate from Ce^{3+} to Tb^{3+} is 25 μs^{-1} (at room temperature). This is much faster than the radiative rate of Tb^{3+}.[40] As a result, the excited state of Tb^{3+} ($^5D_4$) can be populated many times by energy transfer from Ce^{3+} before the depopulation occurs, which result in the increase of emission intensity during this period. Thus, the emission characteristics of Ce^{3+} and Tb^{3+} in Figure 8 can be understood.

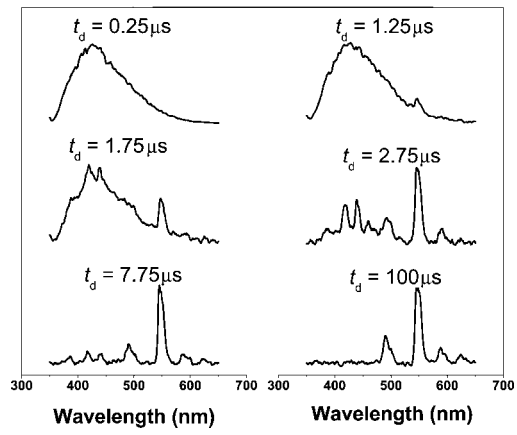

Figure 8. Time-resolved PL spectra of $SiO_2@Y_{1.84}Ce_{0.06}Tb_{0.1}SiO_5$ core/shell particles (λ_{ex} = 370 nm).

A summary of the emission and energy-transfer processes in $SiO_2@Y_{1.84}Ce_{0.06}Tb_{0.1}SiO_5$ is shown schematically in Figure 9.[41] An electron on Ce^{3+} ion is excited from the ground state (4f) to the excited state (5d) by UV light. In the excited state, this electron either relaxes to the lowest 5d crystal-field-splitting state then returns to the ground state to produce the blue emission, or transfers its excitation energy to the higher excited energy levels of Tb^{3+} ($4f^8$), which relax to the $^5D_4$ level, where the green emission ($^5D_4 \rightarrow {}^7F_J$) takes place.[41] Competition between the above two processes results in the occurrence of emission from Ce^{3+} and Tb^{3+} simultaneously in $SiO_2@Y_{1.84}Ce_{0.06}Tb_{0.1}SiO_5$ (Figure 9, b)

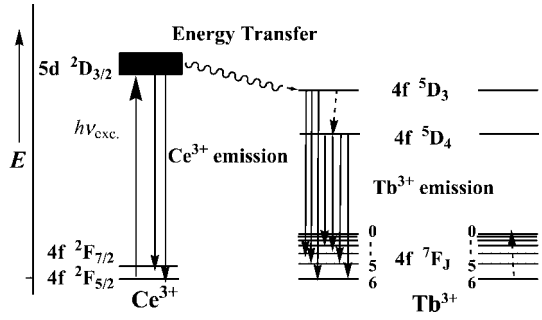

Figure 9. Scheme of energy transfer from Ce^{3+} to Tb^{3+}.

Cathodoluminescence Properties

Similar to the emission under UV excitation, the $SiO_2@Y_{1.9}Tb_{0.1}SiO_5$, $SiO_2@Y_{1.94}Ce_{0.06}SiO_5$, and $SiO_2@Y_{1.84}Ce_{0.06}Tb_{0.1}SiO_5$ core/shell particles also exhibit strong red-green, blue, and blue-green luminescence, respectively, upon excitation with an electron beam (3 kv). Typical

emission spectra are shown in Figure 10 (a–c), respectively. These emission spectra basically agree with the corresponding PL emission spectra (Figure 4 and Figure 7). The CL emission for SiO_2 particles coated with four layers of $Y_{1.94}Ce_{0.06}SiO_5$, $Y_{1.9}Tb_{0.1}SiO_5$, $Y_{1.84}Ce_{0.06}Tb_{0.1}SiO_5$ were investigated as a function of accelerating voltage, as shown in Figure S6 (a–c, respectively). When the filament is fixed at 14 mA, the CL intensities of $SiO_2@Y_{1.94}Ce_{0.06}SiO_5$, $SiO_2@Y_{1.9}Tb_{0.1}SiO_5$, and $SiO_2@Y_{1.84}Ce_{0.06}Tb_{0.1}SiO_5$ core/shell particles increase upon raising the acceleration voltage from 1 to 5 kV. For cathodoluminescence, the Ce^{3+} and Tb^{3+} ions are excited by the plasmons produced by the incident electrons. The electron penetration depth can be estimated by Equation (4)[42,43]

$$L\,[\text{Å}] = 250\left(\frac{A}{\rho}\right)\left(\frac{E}{Z^{\frac{1}{2}}}\right)^{n} \quad (4)$$

where $n = 1.2/(1 - 0.29\cdot\log_{10} Z)$, and A is the atomic weight, ρ is the density, Z is the atomic number, and E is the accelerating voltage (V).[44] For $SiO_2@X_1$-$Y_2SiO_5:Tb^{3+}$ and $SiO_2@X_1$-$Y_2SiO_5:Ce^{3+}$, the electron penetration depth at 5 kV is 16.5 nm. This value is within the X_1-$Y_2SiO_5:Tb^{3+}$, X_1-$Y_2SiO_5:Ce^{3+}$, and $SiO_2@Y_{1.84}Ce_{0.06}Tb_{0.1}SiO_5$ shell for the $SiO_2@X_1$-$Y_2SiO_5:Tb^{3+}$, $SiO_2@X_1$-$Y_2SiO_5:Ce^{3+}$, and $SiO_2@Y_{1.84}Ce_{0.06}Tb_{0.1}SiO_5$ core/shell particles, respectively. With the increase of accelerating voltage, more plasmons will be produced by the incident electrons, which results in more Ce^{3+} and Tb^{3+}ions being excited and thus a higher CL intensity. The increase in electron energy is attributed to deeper penetration of the electron into the shell, which is governed by Equation (4).

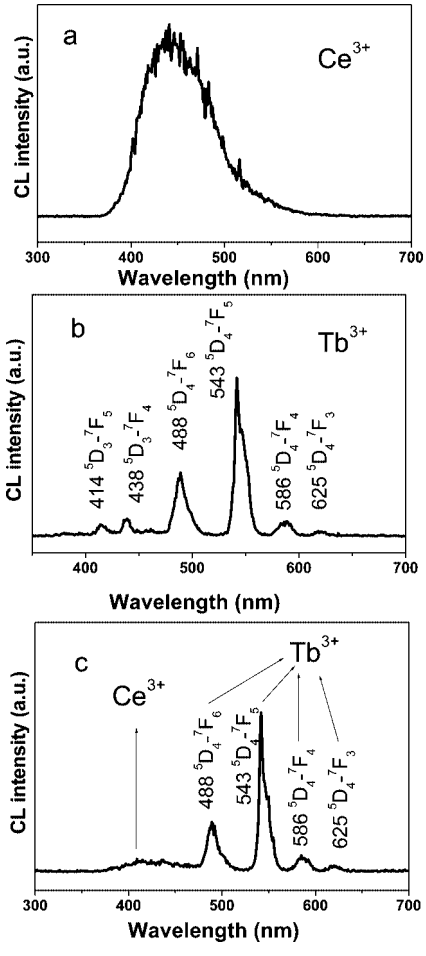

Figure 10. CL spectra of $SiO_2@Y_{1.94}Ce_{0.06}SiO_5$ (a), $SiO_2@Y_{1.9}Tb_{0.10}SiO_5$ (b), and $SiO_2@Y_{1.84}Ce_{0.06}Tb_{0.10}SiO_5$ (c) core/shell particles (voltage: 3 kV).

The deeper penetration of electrons into the shell results in an increase in the electron–solid interaction volume in which excitation of Ce^{3+} and Tb^{3+}ions, which is responsible for light emission, takes place. Therefore, an increase in interaction volume, which effectively determines the generation of light inside the shell, with an increase in electron energy brings about an increase in the CL brightness of $SiO_2@Y_2SiO_5:Tb^{3+}$ and $SiO_2@Y_2SiO_5:Ce^{3+}$ core/shell particles.[45]

Conclusions

A simple and effective sol–gel process has been developed to coat X_1-Y_2SiO_5: RE^{3+} (RE = Eu^{3+}, Ce^{3+}, and/or Tb^{3+}) phosphor layers on monodisperse spherical SiO_2 particles. The obtained $SiO_2@Y_2SiO_5:Eu^{3+}$, $SiO_2@Y_2SiO_5:Tb^{3+}$, $SiO_2@$-$Y_2SiO_5:Ce^{3+}$, and $SiO_2@Y_2SiO_5:Ce^{3+},Tb^{3+}$ core/shell-structured phosphors maintain the spherical morphology, submicrometer size, and narrow size-distribution of the originals. Under the excitation of UV light and electron beams, these core/shell phosphors show red, green, blue, and green luminescence, respectively. An energy transfer from Ce^{3+} to Tb^{3+} exists in $SiO_2@Y_2SiO_5:Ce^{3+},Tb^{3+}$ core/shell phosphors, and this has been studied by time-resolved spectroscopic methods. This process can be extended to prepare other phosphor materials with a homogeneous spherical morphology.

Experimental Section

The core/shell samples with general compositions $SiO_2@Y_{1.8}Eu_{0.2}$-SiO_5, $SiO_2@Y_{1.9}Tb_{0.1}SiO_5$, $SiO_2@Y_{1.94}Ce_{0.06}SiO_5$, and $SiO_2@Y_{1.84}Ce_{0.06}Tb_{0.1}SiO_5$ were prepared by a sol–gel process. The main starting materials were Y_2O_3 (99.99%), Eu_2O_3 (99.99%), $Ce_2(CO_3)_3$ (99.99%), and Tb_4O_7 (99.99%), all of which were purchased from Shanghai Yuelong Nonferrous Metals Limited, tetraethyl orthosilicate $Si(OC_2H_5)_4$ (TEOS, 99 wt.-%, analytical reagent, Beijing Beihua Chemicals Co., Ltd.), polyethylene glycol (PEG, molecular weight 10000, analytical reagent), and ammonium hydroxide (25 wt.-%, analytical reagent, Beijing Beihua Chemicals Co., Ltd.).

First, monodisperse silica spheres were prepared by the well-known Stöber method.[10] In a typical experiment, 7.8 mL of TEOS, 18 mL of deionized H_2O, and 98 mL of NH_4OH were added to 75 mL of absolute ethanol and stirred at room temperature for 3 h to give a white silica colloidal suspension. The silica particles were centrifugally separated from the suspension and washed with ethanol three times. Then, coating of the SiO_2 particles with Y_2SiO_5-based phos-

phor layers was performed by a sol–gel process. According to the compositions in the above formulae, stoichiometric amounts of Y_2O_3, Eu_2O_3, Tb_4O_7, and $Ce_2(CO_3)_3$ were dissolved in dilute HNO_3 with vigorous stirring. Then, a certain amount of TEOS and water/ethanol (v/v = 1:7) was added to the solution and PEG was added with a concentration of 0.1 g/mL. The solution was stirred for 3 h to form a sol, and then silica particles were added with stirring. After stirring for 3 h, the silica particles were separated by centrifugation. The samples were immediately dried at 100 °C for 1 h. The dried samples were annealed to 1000 °C at a heating rate of 2 °C min^{-1} and held there for 2 h in air (for samples containing Eu) or in a reducing atmosphere (CO for samples containing Ce and/or Tb). The above process was repeated several times to increase the thickness of the phosphor shells. For comparison, the coating sol was evaporated in a similar way to produce the pure Y_2SiO_5-based powder phosphors. The whole process is shown schematically in Figure 1.

X-ray diffraction (XRD) studies of the powder samples were performed with a Rigaku-Dmax-IIB spectrometer with using Cu-K_α radiation (λ = 0.15405 nm). The morphology of the samples was inspected with a field emission scanning electron microscope (FE-SEM, XL30, Philips) and a transmission electron microscope (JEOL-2010, 200 kV). The excitation and emission spectra were recorded with a Hitachi F-4500 spectrofluorimeter equipped with a 150-W xenon lamp and 1–6-kv electron gun (self-made) as the excitation source. Luminescence decay curves were obtained with a Lecroy Wave Runner 6100 Digital Oscilloscope (1 GHz) using a 250-nm laser (pulse width: 4 ns, gate: 50 ns) as the excitation source (Continuum Sunlite OPO). All the measurements were performed at room temperature.

Supporting Information (see also the footnote on the first page of this article): Figure S1. Formation process of $SiO_2@Y_2SiO_5:Eu^{3+}$, $SiO_2@Y_2SiO_5:Ce^{3+}$, $SiO_2@Y_2SiO_5:Tb^{3+}$, and $SiO_2@Y_2SiO_5:Ce^{3+},Tb^{3+}$ core/shell particles with the corresponding luminescent photos under UV irradiation. Figure S2. The crystal structure of X_1-Y_2SiO_5. Figure S3. Decay curves for the luminescence of Eu^{3+} in $SiO_2@Y_{1.8}Eu_{0.2}SiO_5$ core/shell particles. Figure S4. Decay curve for the luminescence of Tb^{3+} in $SiO_2@Y_{1.9}Tb_{0.1}SiO_5$ core/shell particles. Figure S5. Decay curves for the luminescence of Ce^{3+} in $SiO_2@Y_{1.94}Ce_{0.06}SiO_5$ (a) and in $SiO_2@Y_{1.84}Ce_{0.06}Tb_{0.1}SiO_5$ (b) core/shell particles. Figure S6. CL emission intensity of $SiO_2@Y_{1.94}Ce_{0.06}SiO_5$ (a) $SiO_2@Y_{1.9}Tb_{0.10}SiO_5$ (b), and $SiO_2@Y_{1.84}Ce_{0.06}$ $Tb_{0.10}SiO_5$ (c) core/shell particles as a function of accelerating voltage. Table S1. Calculated internuclear distances and angles of $SiO_2@Y_2SiO_5$:Tb core/shell particles.

Acknowledgments

This project was financially supported by the "Bairen Jihua" foundation of the Chinese Academy of Sciences, the National Natural Science Foundation of China (50225205, 50572103, and 20431030) and the MOST of China (no. 2003CB314707). Dr M. Yu is grateful for a special starting research fund for awardees of the President Prize of the Chinese Academy of Sciences (2005–2007).

[1] I. L. Radtchenko, G. B. Sukhorukov, N. Gaponik, A. Kornowski, A. L. Rogach, H. Mohwald, *Adv. Mater.* **2001**, *13*, 1684–1687; C. T. Kresge, M. E. Leonowicz, W. J. Roth, J. C. Vartuli, J. S. Beck, *Nature* **1992**, *359*, 710–712; H. Yang, N. Coombs, G. A. Ozin, *Nature* **1997**, *386*, 692–695; D. Zhao, J. Feng, Q. Huo, N. Melosh, G. H. Fredrickson, B. F. Chmelka, G. D. Stucky, *Science* **1998**, *279*, 548–552; P. V. Braun, P. Osenar, S. I. Stupp, *Nature* **1996**, *380*, 325–328; J. Liu, Y. Shin, Z. Nie, J. H. Chang, L. Q. Wang, G. E. Fryxell, W. D. Samuels, G. J. Exarhos, *J. Phys. Chem. A* **2000**, *104*, 8328–8339; C. W. Guo, Y. Cao, S. H. Xie, W. L. Dai, K. N. Fan, *Chem. Commun.* **2003**, 700–701.

[2] J. J. Schneider, *Adv. Mater.* **2001**, *13*, 529–533; C. J. Zhong, M. M. Maye, *Adv. Mater.* **2001**, *13*, 1507–1511; M. S. Fleming, T. K. Mandal, D. R. Walt, *Chem. Mater.* **2001**, *13*, 2210; M. Yu, J. Lin, J. Fang, *Chem. Mater.* **2005**, *17*, 1783–1791.

[3] J. H. Lee, T. G. Park, H. K. Choi, *J. Microencapsulation* **1999**, *16*, 715–729; R. Schirrer, R. Lenke, J. Boudouaz, *Polym. Eng. Sci.* **1997**, *37*, 1748–1760.

[4] C. Louis, S. Roux, G. Ledoux, L. Lemelle, P. Gillet, O. Tillement, P. Perriat, *Adv. Mater.* **2004**, *16*, 2163–2166.

[5] Z. J. Jiang, C. Y. Liu, *J. Phys. Chem. B* **2003**, *107*, 12411; H. Giesche, E. Matijevic, *J. Mater. Res.* **1994**, *9*, 436–450.

[6] R. A. Caruso, M. I. Antoniett, *Chem. Mater.* **2001**, *13*, 3272–3282.

[7] X. Jing, T. G. Ireland, C. Gibbons, D. J. Barber, J. Silver, A. Vecht, G. Fern, P. Trogwa, D. Morton, *J. Electrochem. Soc.* **1999**, *146*, 4654–4658; A. Vecht, C. Gibbons, D. Davies, X. Jing, P. Marsh, T. G. Ireland, J. Silver, A. Newport, *J. Vac. Sci. Technol. B* **1999**, *17*, 750–757; Y. D. Jiang, Z. L. Wang, F. Zhang, H. G. Paris, C. J. Summers, *J. Mater. Res.* **1998**, *13*, 2950–2955.

[8] Y. H. Zhou, J. Lin, X. M. Han, S. B. Wang, H. J. Zhang, *Mater. Res. Bull.* **2003**, *38*, 1289–1299; S. H. Cho, J. S. Yoo, J. D. Lee, *J. Electrochem. Soc.* **1998**, *145*, 1017–1019.

[9] A. Celikkaya, M. Akinc, *J. Am. Ceram. Soc.* **1990**, *73*, 2360–2365.

[10] W. Stöber, A. Fink, *J. Colloid Interf. Sci.* **1968**, *26*, 62–69; G. H. Bogush, M. A. Tracy, C. F. Zukoskiiv, *J. Non-Cryst. Solids* **1988**, *104*, 95–106.

[11] J. Lin, Q. Su, S. B. Wang, H. J. Zhang, *J. Mater. Chem.* **1996**, *6*, 265–269; Q. Y. Zhang, K. Pita, W. Ye, W. X. Que, C. H. Kam, *Chem. Phys. Lett.* **2002**, *356*, 161–167; Y. Liu, C. N. Xu, H. Matsui, T. Imamura, T. Watanabe, *J. Lumin.* **2000**, *87*, 1297–1299; S. H. Shin, D. Y. Jeon, K. S. Suh, *Jpn. J. Appl. Phys.* **2001**, *40*, 4715–4719; M. Yin, W. Zhang, L. Lou, S. Xia, J.-C. Krupa, *Physica B* **1998**, *254*, 141–147.

[12] C. Cannas, M. Mainas, A. Musinu, G. Piccaluga, A. Speghini, M. Bettinelli, *Opt. Mater.* **2005**, *27*, 1506–1510.

[13] A. Sennaroglu, *Prog. Quantum Electron.* **2002**, *26*, 287–352; M. Yin, C. K. Duan, W. P. Zhang, S. D. Xia, J. C. Krupa, *J. Appl. Phys.* **1999**, *86*, 3751–3757; W. P. Zhang, P. B. Xie, C. K. Duan, K. Yan, M. Yin, L. R. Lou, S. D. Xia, J. C. Krupa, *Chem. Phys. Lett.* **1998**, *292*, 133–136; M. Yin, W. P. Zhang, L. R. Lou, S. D. Xia, J. C. Krupa, *Spectrosc. Lett.* **1998**, *31*, 767–778; M. Yin, W. P. Zhang, S. D. Xia, J. C. Krupa, *J. Lumin.* **1996**, *68*, 335–339.

[14] T. Aitasalo, J. Holsa, M. Lastusaari, J. Niittykoski, F. Pelle, *Opt. Mater.* **2005**, *27*, 1511–1515; C. Li, C. Wyon, R. Moncorge, *IEEE J. Quantum Electron.* **1992**, *28*, 1209–1221.

[15] T. E. Peters, *J. Electrochem. Soc.* **1969**, *116*, 985–989; H. S. Kang, Y. C. Kang, H. D. Park, Y. G. Shul, *Appl. Phys. A* **2005**, *80*, 347–351.

[16] M. Mitsunaga, R. Yano, N. Uesugi, *Opt. Lett.* **1991**, *16*, 1890–1892; R. Yano, M. Mitsunaga, N. Uesugi, *J. Opt. Soc. Am. B – Opt. Phys.* **1992**, *9*, 992–997.

[17] N. F. M. Henry, K. Lonsdale, *International Tables for X-ray Crystallography*, vol. 1, Kynoch Press, Birmingham UK, **1952**.

[18] J. Felsche, *Struct. Bond.* **1973**, *13*, 99; J. Ito, H. Johnson, *Am. Miner.* **1968**, *53*, 1940–1946.

[19] T. Aitasalo, J. Holsa, M. Lastusaari, J. Niittykoski, F. Pelle, *Opt. Mater.*, in press.

[20] J. G. Wang, S. J. Tian, G. B. Li, F. H. Liao, X. P. Jing, *Mater. Res. Bull.* **2001**, *36*, 1855–1861.

[21] L. S. Birks, H. Friedman, *J. Appl. Phys.* **1946**, *17*, 687–692.

[22] M. D. Segall, P. L. D. Lindan, M. J. Probert, C. J. Pickard, P. J. Hasnip, S. J. Clark, M. C. Payne, *J. Phys.: Condens. Matter* **2002**, *14*, 2717–2744.
[23] C. Louis, K. Lebbou, M. A. Flores-Gonzalez, R. Bazzi, B. Hautefeuille, B. Mercier, S. Roux, P. Perriat, C. Olagnon, O. Tillement, *J. Crystal Growth* **2004**, *265*, 459–465; C. Louis, R. Bazzi, M. A. Flores-Gonzalez, W. Zheng, K. Lebbou, O. Tillement, B. Mercier, C. Dujardin, P. Perriat, *J. Solid State Chem.* **2003**, *173*, 335–341; G. Ledoux, B. Mercier, C. Louis, C. Dujardin, O. Tillement, P. Perriat, *Radiation Measurements* **2004**, *38*, 763–766.
[24] C. Duan, M. Yin, K. Yan, M. F. Reid, *J. Alloy Comput.* **2000**, *303–305*, 371–375; C. Duan, S. Xia, W. Zhang, M. Yin, J.-C. Krupa, *J. Alloy Comput.* **1998**, *275–277*, 450–454.
[25] M. Yu, J. Lin, J. Fu, H. J. Zhang, Y. C. Han, *J. Mater. Chem.* **2003**, *13*, 1413–1419.
[26] R. C. G. Naber, P. W. M. Blom, G. H. Gelinck, A. W. Marsman, D. M. de Leeuw, *Adv. Mater.* **2005**, *17*, 2692–2695.
[27] C. Peng, H. Zhang, J. Yu, Q. Meng, L. Fu, H. Li, L. Sun, X. Guo, *J. Phys. Chem. B* **2005**, *109*, 15278–15287.
[28] T. Yamase, T. Kobayashi, M. Sugeta, H. Naruke, *J. Phys. Chem. A* **1997**, *101*, 5046–5053.
[29] M. H. V. Werts, R. T. F. Jukes, J. W. Verhoeven, *Phys. Chem. Chem. Phys.* **2002**, *4*, 1542–1548.
[30] M. Sugeta, T. Yamase, *Bull. Chem. Soc. Jpn.* **1993**, *66*, 444–449.
[31] L. D. Carlos, Y. Messadeq, H. F. Brito, R. A. Sa-Ferreira, V. de Zea Bermudz, S. J. L. Ribeiro, *Adv. Mater.* **2000**, *12*, 594–598.
[32] M. F. Hazenkamp, G. Blasse, *Chem. Mater.* **1990**, *2*, 105–110.
[33] S. J. L. Ribeiro, K. Dahmouche, C. A. Ribeiro, C. V. Santilli, S. H. J. Pulcinelli, *J. Sol-Gel Sci. Technol.* **1998**, *13*, 427–432.
[34] T. R. Zhang, C. Spitz, M. Antonietti, C. F. J. Faul, *Chem. Eur. J.* **2005**, *11*, 1001–1009.
[35] See ref. 19.
[36] M. Yu, J. Lin, J. Fu, Y. C. Han, *Chem. Phys. Lett.* **2003**, *371*, 178–183.
[37] G. Blasse, A. Bril, *J. Chem. Phys.* **1967**, *47*, 1920–1926.
[38] V. A. Pustovarov, B. V. Shulgin, S. A. Smirnov, E. I. Zinin, *Nucl. Instrum. Methods Phys. Res., Sect. A* **1998**, *405*, 396–399.
[39] I. M. Batayev, S. U. Morev, *Opt. Spectrosk.* **1966**, *80*, 85–89.
[40] W. van Schaik, S. H. M. Poort, J. J. H. Schlotter, E. Dorrestijn, G. Blasse, *J. Electrochem. Soc.* **1994**, *141*, 2201–2207.
[41] M. T. Jose, A. R. Lakshmanan, *Opt. Mater.* **2004**, *24*, 651–659; J.-C. Bourcet, F. K. Fong, *J. Chem. Phys.* **1974**, *60*, 34–39; Z. L. Wang, Z. W. Quan, J. Lin, J. Fang, *J. Nanosci. Nanotech.* **2005**, *5*, 1532–1536.
[42] H. A. Bette, *Ann. Phys. (Leipzig)* **1930**, *5*, 325.
[43] H. Wang, C. K. Lin, X. M. Liu, J. Lin, M. Yu, *Appl. Phys. Lett.* **2005**, *87*, 181907.
[44] C. Feldman, *Phys. Rev.* **1960**, *117*, 455–459.
[45] D. Kumar, K. G. Cho, Z. Chen, V. Craciun, P. H. Holloway, R. K. Singh, *Phys. Rev. B* **1999**, *60*, 13331–13334.

Received: March 24, 2006
Published Online: August 2, 2006

